Report

Neuron

White-Matter Tract Connecting Anterior Insula to Nucleus Accumbens Correlates with Reduced Preference for Positively Skewed Gambles

Highlights

- A novel tract connecting the anterior insula to the NAcc was traced and validated
- Tract coherence correlated with reduced preference for positively skewed gambles
- NAcc activity before risky choice mediated the association of structure with behavior

Authors

Josiah K. Leong, Franco Pestilli, Charlene C. Wu, Gregory R. Samanez-Larkin, Brian Knutson

Correspondence

knutson@psych.stanford.edu

In Brief

Leong et al. identify a white-matter tract connecting the anterior insula and nucleus accumbens. The tract's coherence is associated with reduced preference for positively skewed gambles. NAcc neural activity before choice statistically accounted for the association of structure with behavior.

Leong et al., 2016, Neuron *89*, 63–69
January 6, 2016
http://dx.doi.org/10.1016/j.neuron.2015.12.015

CellPress

Neuron
Report

White-Matter Tract Connecting Anterior Insula to Nucleus Accumbens Correlates with Reduced Preference for Positively Skewed Gambles

Josiah K. Leong,[1] Franco Pestilli,[2] Charlene C. Wu,[1] Gregory R. Samanez-Larkin,[3] and Brian Knutson[1,4,*]
[1]Department of Psychology, Stanford University, Stanford, CA 94305, USA
[2]Department of Psychological and Brain Sciences, Indiana University, Bloomington, IN 47405, USA
[3]Department of Psychology, Yale University, New Haven, CT 06520, USA
[4]Stanford Neuroscience Institute, Stanford University, Stanford, CA 94305, USA
*Correspondence: knutson@psych.stanford.edu
http://dx.doi.org/10.1016/j.neuron.2015.12.015

SUMMARY

Individuals sometimes show inconsistent risk preferences, including excessive attraction to gambles featuring small chances of winning large amounts (called "positively skewed" gambles). While functional neuroimaging research indicates that nucleus accumbens (NAcc) and anterior insula (AIns) activity inversely predict risky choice, structural connections between these regions have not been described in humans. By combining diffusion-weighted MRI with tractography, we identified the anatomical trajectory of white-matter tracts projecting from the AIns to the NAcc and statistically validated these tracts using Linear Fascicle Evaluation (LiFE) and virtual lesions. Coherence of the right AIns-NAcc tract correlated with reduced preferences for positively skewed gambles. Further, diminished NAcc activity during gamble presentation mediated the association between tract structure and choice. These results identify an unreported tract connecting the AIns to the NAcc in humans and support the notion that structural connections can alter behavior by influencing brain activity as individuals weigh uncertain gains against uncertain losses.

INTRODUCTION

Choice consistency is a hallmark of rationality (von Neumann and Morgenstern, 1944). Nonetheless, people sometimes choose inconsistently in predictable ways (Kahneman and Tversky, 1979). For instance, the profitability of casinos and lotteries suggests that people are seduced by "positively skewed" gambles that feature a small chance of winning a large amount combined with a large chance of losing a little (Kraus and Litzenberger, 1976). Neuroimaging experiments suggest that, when presented with positively skewed gambles, people report experiencing greater positive arousal (e.g., feelings akin to "excitement") and show increased brain activity in circuits associated with gain anticipation, including the nucleus accumbens (or NAcc), which might encourage risk taking (Wu et al., 2011).

Recent advances in neuroimaging have allowed researchers to visualize brain activity that not only correlates with presentation of risky options, but that also precedes and predicts choice among them (Knutson and Bossaerts, 2007). For instance, using fMRI, researchers have shown that increased NAcc activity predicts risk-seeking choices, but increased anterior insula (AIns) activity predicts risk-averse choices on a trial-to-trial basis (e.g., Kuhnen and Knutson, 2005). Comparative research suggests that these regions receive input from evolutionarily conserved dopaminergic and noradrenergic projections emanating from the midbrain, respectively, and theorists have speculated that release of these neurotransmitters in relevant terminal regions may promote approach or avoidance behavior (e.g., Knutson et al., 2014; Panksepp, 1998).

Although fMRI can provide information about which brain circuits promote choice, it cannot illuminate the structural connections between those circuits. Recently, investigators have used diffusion-weighted imaging (DWI) to trace ascending mesolimbic axonal projections from the ventral tegmental area to the NAcc, as well as descending projections from the medial prefrontal cortex (MPFC) to the NAcc (Coenen et al., 2012; Cohen et al., 2008; Draganski et al., 2008; Lehéricy et al., 2004), recapitulating anatomical tracing studies of nonhuman primates (reviewed in Haber and Knutson, 2010). Diffusion measures such as fractional anisotropy (FA) have been associated with white-matter density, alignment, and diameter (collectively referred to as "coherence" henceforth; Jones et al., 2013). Assuming that greater white-matter coherence promotes the transmission of functional signals, higher coherence might modulate brain activity in specific projection target regions, which might then influence behavior. For instance, the coherence of white-matter projections from the MPFC to the NAcc can account for individual differences in reward learning (Samanez-Larkin et al., 2012).

Whereas investigators have used DWI to estimate the coherence of prefrontal projections to the NAcc, other projections might also modulate NAcc activity. For instance, activity in both the NAcc and AIns precedes, but has opposing effects on, risky choice (Kuhnen and Knutson, 2005). To date, direct structural connections between the AIns and NAcc have not been documented in humans. Only two studies in other species

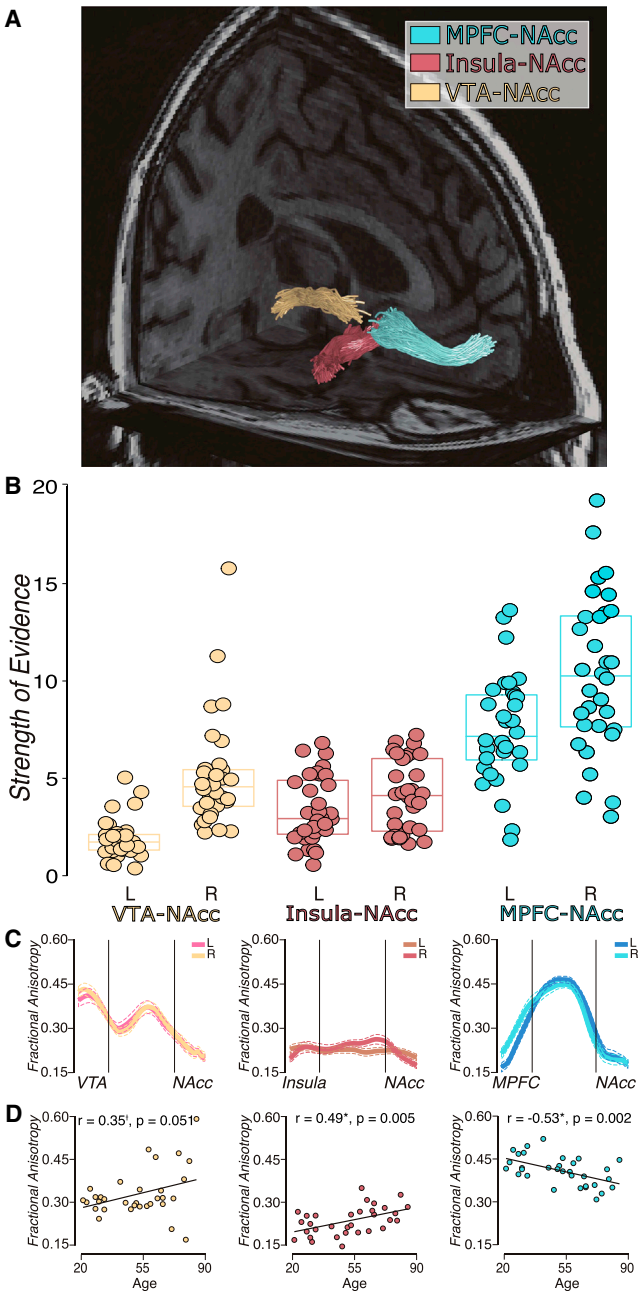

Figure 1. Trajectory and Validation of White-Matter Tracts

(A) Anatomy. White-matter tracts identified in a representative right hemisphere dataset.

(B) Statistical validation. Strength of evidence for the tracts in each individual brain (circles), with group median and interquartile-range boxplot (Supplemental Information).

(C) White-matter coherence along tract length. FA profiles for each tract, depicting mean FA and SE across individual brains (vertical bars delineate the middle 50% of nodes included in analyses in D).

(D) Associations of age with tract coherence replicated and extended previous findings (Supplemental Information).

have suggested the possibility of such a connection (Chikama et al., 1997; Reynolds and Zahm, 2005). While tracers implicated unidirectional glutamatergic projections from the AIns to the NAcc, the researchers could only visualize the destination but not the spatial trajectories of projections.

We investigated whether similar tracts project from the AIns to the NAcc in humans. Further, we explored whether the white-matter coherence of identified tracts might account for brain activity as well as behavior related to gambles. Since functional neuroimaging studies suggest that positively skewed gambles preferentially increase NAcc activity (Wu et al., 2012), we predicted that the coherence of an AIns-NAcc tract might decrease NAcc activity and choices of positively skewed gambles. We also tested for a more prominent association in the right hemisphere, since right AIns activity most consistently correlates with negative arousal and risk perception (Craig, 2009; Critchley et al., 2001; Paulus et al., 2003).

RESULTS

Analyses first identified and validated a white-matter tract connecting the AIns and NAcc, next verified previously documented mesolimbic white-matter tracts, then characterized functional predictors of positive-skew preference during a gambling task, and finally tested whether functional activity could account for the association of tract coherence with positive-skew preference.

Identification and Validation of White-Matter Tracts Connecting the AIns and NAcc

Probabilistic tractography identified three bilateral white-matter tracts in all subjects' brains (n = 32; Figure 1A). One pair of tracts projected through the subcaudate white matter from the AIns to the NAcc (Figure S1). Two other pairs of tracts projected from the MPFC to the NAcc and between the VTA and the NAcc, replicating previously described pathways (Samanez-Larkin et al., 2012).

Statistical evidence for these tracts was evaluated using the Linear Fascicle Evaluation method and virtual lesions approach (LiFE; Pestilli et al., 2014). Results revealed strong statistical evidence for the existence of all three bilateral tracts (i.e., connecting the AIns and NAcc, MPFC and NAcc, and VTA and NAcc; Figure 1B). FA was computed based on a standard tensor model (Basser and Pierpaoli, 1996) to index white-matter coherence for each tract. Each tract's FA profile was computed across each tract in each hemisphere and subject and then averaged across the middle 50% portion of each tract's profile to index coherence (Figure 1C; Supplemental Information). Effects of age on FA replicated and extended previous findings (Samanez-Larkin et al., 2012; Figure 1D; Supplemental Information).

Association of AIns to NAcc Tract Coherence with Reduced Positive-Skew Preference

Risk preference for all three gamble conditions and tract coherence for all three bilateral tracts were submitted to a repeated-measures multivariate analysis of variance, which revealed a significant tract by condition interaction for the AIns-NAcc bilateral tract (right: $F(2,50) = 4.10$, $p = 0.023$,

Table 1. Logistic Regression Results, Including Subjects as Random Effects

Variable	Contrast	Behavioral Model	Neural Model	Combined Model
Previous gamble outcome	gain > loss	−2.19* (−0.14, 0.06)		−2.55* (−0.17, 0.07)
	accept > reject	1.53 (0.13, 0.09)		2.01* (0.18, 0.09)
Domain of current earnings	loss	1.51 (0.40, 0.26)		1.71 (0.45, 0.26)
	gain	1.35 (0.35, 0.26)		1.52 (0.39, 0.26)
Skewness	positive > negative	6.16*** (0.36, 0.06)		5.50*** (0.32, 0.06)
	skewed > symmetric	−5.61*** (−0.49, 0.09)		−5.86*** (−0.52, 0.09)
Right NAcc			4.96*** (0.63, 0.13)	5.09*** (0.67, 0.13)
Right AIns			−3.30*** (−0.39, 0.12)	−3.00** (−0.36, 0.12)
Right MPFC			3.70*** (0.35, 0.10)	3.50*** (0.34, 0.10)
Pseudo R^2		0.27	0.27	0.30
AIC		2,644	2,666	2,594
BIC		2,689	2,695	2,657

Based on AIC, BIC, and a likelihood-ratio test for nested models, the best model for predicting trial-by-trial risky choice includes terms for right hemisphere neural activity, gamble type, previous gamble outcome, and domain of current earnings ($\chi^2(3) = 55.32$, $p < 0.0001$). Winning a previous gamble significantly predicted risk aversion on the following trial. A model including left-hemisphere neural activity did not improve model fit (Table S3). Z scores are shown with coefficient estimates and SE in parentheses. ***$p < 0.001$, **$p < 0.01$, *$p < 0.05$.

$\eta^2 = 0.634$; left: $F(2,50) = 4.69$, $p = 0.014$, $\eta^2 = 0.726$; Table S1). We additionally found a significant effect of gamble condition on risk seeking ($F(2,50) = 4.01$, $p = 0.024$, $\eta^2 = 0.622$). Pairwise comparisons revealed that subjects who did not always choose to seek or avoid risk for any gamble condition (n = 20) preferred positively skewed to negatively skewed gambles (paired $t(19) = 2.13$, $p = 0.047$). This preference, however, varied across individuals (Figure S2).

Pairwise correlations showed that individual differences in right hemisphere AIns-NAcc tract coherence were associated with reduced preference for positively skewed gambles ($\beta = -0.40$, $t(30) = -2.38$, $p = 0.02$). This association remained significant after controlling for age and multiple comparisons for testing bilateral tracts ($\beta = -0.44$, $t(30) = -2.37$, $p = 0.02$). Further, this association remained robust after removing seven subjects who either never (n = 3) or always (n = 4) took positively skewed gambles ($\beta = -0.47$, $t(23) = -2.57$, $p = 0.02$). Right AIns-NAcc tract coherence was also marginally negatively associated with general risk taking across all gamble conditions ($\beta = -0.31$, $t(30) = -1.80$, $p = 0.08$), but not specifically for symmetric ($\beta = -0.08$, $t(30) = -0.46$, $p = 0.65$) or negative-skew ($\beta = -0.14$, $t(30) = -0.77$, $p = 0.45$) gambles. Left-hemisphere AIns-NAcc tract coherence was marginally associated with decreased risk taking for negatively skewed gambles ($\beta = -0.34$, $t(30) = -2.03$, $p = 0.06$), but not with risk taking in general or any other gamble condition (positive skew: $\beta = -0.10$, $t(30) = -0.54$, $p = 0.59$; symmetric: $\beta = -0.02$, $t(30) = -0.09$, $p = 0.93$; overall: $\beta = -0.23$, $t(30) = -1.27$, $p = 0.21$). Coherence of other tracts (i.e., the bilateral MPFC-NAcc tract and bilateral VTA-NAcc tract) was not associated with risk taking in general or in any gamble condition.

Association of Functional Brain Activity with Risky Choice

fMRI data were preprocessed and activity time courses extracted from predefined volumes of interest (Experimental Procedures). Logistic regressions indicated that activity immediately preceding choice predicted risk taking on a trial-to-trial basis within subjects. Specifically, right NAcc and MPFC activity predicted risk-seeking choices, whereas right AIns activity predicted risk-averse choices across all gambles (Table 1). Gamble type also predicted risk-seeking choices. These variables predicted choices to gamble even after controlling for other potentially relevant variables (e.g., the previous gamble's outcome, domain of current earnings relative to one's endowment). The best-fitting model included right hemisphere neural activity, gamble type, previous gamble outcome, and domain of current earnings (indicated by Akaike Information Criterion [AIC], Bayesian Information Criterion [BIC], and a likelihood-ratio test: $\chi^2(3) = 55.32$, $p < 0.0001$; Table 1).

Activity time courses were plotted and analyzed to verify that gamble type differentially altered neural activity in volumes of interest in a way that could influence choice. Findings indicated that presentation of positively skewed gambles elicited greater activity in the right and left NAcc prior to choice than did symmetric or negatively skewed gambles (right: positive skew > symmetric: $t(31) = 2.17$, $p = 0.04$; positive skew > negative skew: $t(31) = 2.80$, $p = 0.01$; left: positive skew > symmetric: $t(31) = 2.87$, $p = 0.01$; positive skew > negative skew: $t(31) = 3.02$, $p = 0.005$), but not in the AIns or MPFC (Figure 2).

Functional Mediation of the Association of Tract Coherence with Reduced Positive-Skew Preference

Individual differences in average right NAcc activity immediately prior to choice were entered as a statistical mediator of the association of right AIns-NAcc tract coherence with reduced preference for positively skewed gambles. Results from hierarchical regression analyses indicated that right AIns-NAcc tract coherence was associated with decreased right NAcc activity before gamble choice ($\beta = -0.35$, $p = 0.03$) and that right NAcc activity before gamble choice was associated with individual differences in positive-skew preference ($\beta = 0.46$, $p = 0.003$; Figure 3).

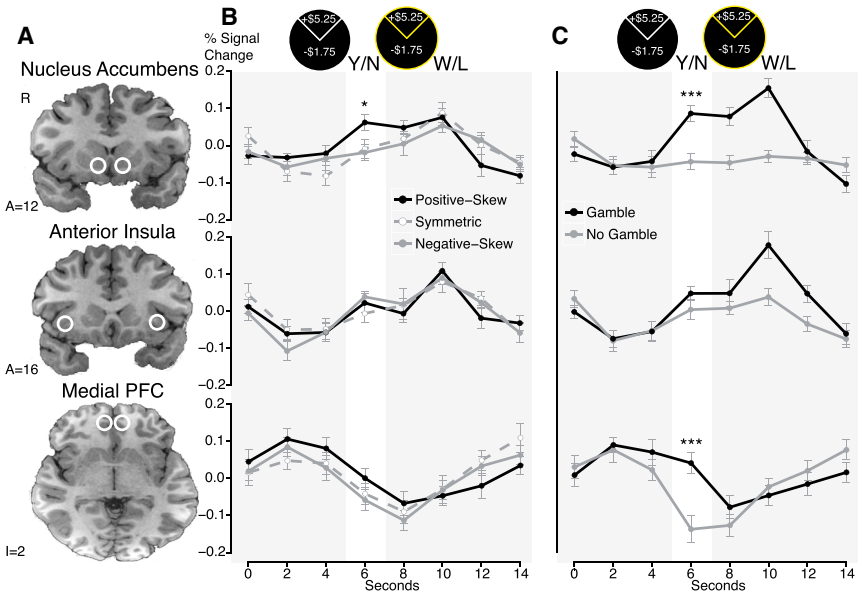

Figure 2. fMRI Activity Time Courses during Gambling Task

(A) Spherical volumes of interest (VOIs) used to obtain activity time course data.

(B) Mean activity and SEs plotted for each right hemisphere VOI by gamble condition. Positively skewed gambles elicited greater NAcc activity than symmetric and negatively skewed gambles during gamble choice (positive skew > symmetric: paired $t(31) = 2.17$, $p = 0.04$; positive skew > negative skew: paired $t(31) = 2.80$, $p = 0.01$).

(C) Right NAcc and MPFC activity were greater for accepted than rejected gambles across conditions (NAcc: paired $t(31) = 4.27$, $p = 0.0002$; MPFC: paired $t(31) = 4.06$, $p = 0.0003$). Left-hemisphere VOIs showed similar results (Figure S3).

Importantly, including the indirect effect of right NAcc activity before choice significantly decreased the direct association of right AIns-NAcc tract coherence with reduced positive-skew preference to nonsignificance ($\beta' = -0.24$, $p = 0.14$; $\beta = -0.40$, $p = 0.02$), consistent with statistical mediation. Additional mediation models specified with different terms (i.e., coherence of control tracts and activity of control volumes of interest) established that only right AIns-NAcc tract coherence and right NAcc activity before gamble choice were associated with positive-skew preference (Table S4). Further, confirmatory analyses of an independent fMRI dataset showed that functional coupling of the AIns and NAcc was associated with decreased positive-skew preference (Figure S4).

DISCUSSION

This research identifies an unreported white-matter tract connecting the AIns to the NAcc in humans. Consistent with a potential role in risk preferences, individual differences in AIns to NAcc tract coherence were associated with reduced preference for positively skewed gambles. Functionally, presentation of positively skewed gambles preferentially increased NAcc activity, which predicted subsequent risky choice. Decreased NAcc activity could statistically account for the association of AIns-NAcc tract coherence with reduced preference for positively skewed gambles, forging links from brain structure to brain function to behavior.

These findings illustrate the importance of leveraging comparative neuroanatomy to guide the discovery and characterization of structural connections in humans (e.g., Haber and Knutson, 2010). Only two comparative studies in monkeys and rats had previously suggested that a unidirectional glutamatergic projection existed from the AIns to the NAcc (Chikama et al., 1997; Reynolds and Zahm, 2005). Inspired by those findings, we were able to identify and trace the trajectory of AIns-NAcc tracts in humans. In addition, previously documented tracts (i.e., from the MPFC to the NAcc and connecting the midbrain and NAcc) were validated with novel methods, and their associations with age extended previous findings (Supplemental Information). Thus, structural tracings in animals can provide unique clues not only about where tracts begin and end, but also about their direction and chemical transmission, which can guide interpretations of findings in humans (e.g., Heimer et al., 1991; Lehman et al., 2011).

This investigation also illustrates how multimodal imaging can illuminate new discoveries about brain activity and behavior. The combination of DWI, fMRI, and behavior allowed us to trace a path from brain structure to brain function to behavior. While previous fMRI research suggests that increased NAcc activity promotes financial risk seeking while increased AIns activity instead promotes financial risk aversion (e.g., Kuhnen and Knutson, 2005), the present research begins to situate those findings within an anatomical framework. Specifically, increased AIns to NAcc coherence appeared to reduce preference for positively skewed gambles by decreasing NAcc activity during gamble presentation. Positively skewed gambles preferentially elevated NAcc activity, despite having the same expected value and variance as symmetric and negatively skewed gambles, which might account for the excessive but irrational attractiveness of these "lottery"-like gambles (Wu et al., 2012). Interestingly, by reducing NAcc activity to positively skewed gambles, the coherence of direct projections from the AIns to the NAcc might "rationalize" risky choice, even in the absence of modulation from more "reflective" prefrontal input.

Importantly, current tractography methods cannot quantify differential contributions of crossing fibers within a voxel (Jones et al., 2013). The AIns to NAcc tract traverses the lateral-medial axis of the brain, thereby intersecting with other tracts like the uncinate fasciculus in some subjects (Petrides and Pandya, 2007). Future research with improved methods will therefore need to determine the extent to which the AIns to NAcc tract represents a distinct component of the subcaudate white matter.

Together, these findings provide multimodal empirical support for an "Affect-Integration-Motivation" or AIM framework, which describes choice as arising from hierarchical processes of affective evaluation, integration, and motivation (Samanez-Larkin and

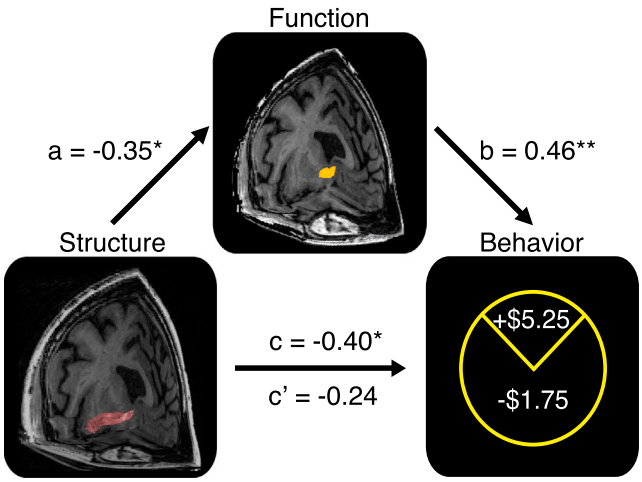

Figure 3. NAcc Functional Activity Mediated the Association between AIns-NAcc Tract Coherence and Positive-Skew Preference

AIns-NAcc tract coherence is associated with reduced NAcc activity during presentation of positively skewed gambles ($\beta = -0.35$, $p = 0.03$), and NAcc activity was associated with positive-skew preference ($\beta = 0.46$, $p = 0.003$). This indirect pathway mediated the association of tract coherence with positive-skew preference ($\beta' = -0.24$, $p = 0.14$; $\beta = -0.40$, $p = 0.02$). Path coefficients are standardized βs. No alternative combination of tract coherence and functional activity could reproduce this pattern of associations (Table S4).

Knutson, 2015). While the connections explored here pertain primarily to affective evaluation, future studies may focus on the connectivity of higher order components of the framework that can support value integration and motivation. The findings also add structural connectivity information to a growing functional neuroimaging literature implicating the NAcc in assessment of expected value, but the AIns in the assessment of risk (Knutson and Bossaerts, 2007; Mohr et al., 2010; Wu et al., 2012), in both financial and other uncertain choices (e.g., Sanfey, 2007). While cross-sectional mediation analysis can only model correlations between brain structure, function, and behavior, these findings also cohere with causal evidence indicating that AIns lesions (which should disconnect projections to the NAcc) can increase financial risk taking (Clark et al., 2008), as well as selectively impair loss but not gain learning (Palminteri et al., 2012).

These multimodal findings highlight new directions for physiological research. Although the findings are logically consistent with repeated demonstrations that NAcc fMRI activity promotes risky choice, it is not clear how glutamatergic projections from the AIns to NAcc might decrease fMRI activity in the NAcc. While comparative research suggests that phasic dopamine release may increase fMRI blood oxygen level-dependent (or BOLD) activity in the NAcc (Choi et al., 2006; Knutson and Gibbs, 2007), the influence of glutamate release on NAcc BOLD activity has not been characterized. One counterintuitive possibility raised by these findings is that glutamate release in the NAcc may interfere with or even decrease dopamine-elicited increases in BOLD activity, consistent with recent findings that combine optogenetics with fMRI (E.A. Ferenczi et al., personal communication).

Identification of a new tract naturally raises many questions for exploration. The anatomical connectivity of the rest of the insular cortex is ripe for additional characterization. Comparative studies suggest that projections from the posterior insula target regions in the AIns, possibly providing peripheral physiological input to affective responses (Chang et al., 2013; Craig, 2009). The AIns also directly connects to lateral cortical regions implicated in controlling and changing the course of action (Aron et al., 2007). Little is known about the trajectory or malleability of these white-matter tracts in humans, and rich opportunities exist for exploring changes in their coherence as a result of gradual (e.g., related to maturation and aging) or more rapid (e.g., experience and training) influences. Perhaps most tantalizing, identification and assessment of the stable properties of tracts may open the door to exploring how targeted interventions can alter their structure and related functions.

EXPERIMENTAL PROCEDURES

Thirty-seven right-handed healthy adults completed the study. Five were excluded from analyses because of head motion >2 mm during the fMRI scan, leaving a total of 32 subjects (14 females, age mean = 52, SD = 19.3, range = 21–85 years). The study was conducted at the Stanford Center for Cognitive and Neurobiological Imaging. Written informed consent was obtained from all subjects prior to participation. Subjects completed behavioral and self-report measures, including neuropsychological tests. Subjects then underwent functional and structural MRI scans and received $20 per hour plus the total earned on the gambling task. The study was approved by the Stanford Institutional Review Board.

Behavioral Task and Analysis

Subjects were scanned with fMRI as they performed a modified version of a gambling task (Wu et al., 2011) during which they made a series of choices to gamble (Figure S2). During each trial (n = 72; 24 per condition), gambles were depicted as circles with slices representing the probability of associated outcomes. If subjects chose to accept, the gamble's outcome was displayed as feedback that cumulated to a final payout, but if they chose to reject, no outcome accrued, which was also displayed as feedback. When prompted with the word "choose," subjects indicated their choices with a left or right button press (spatially counterbalanced across trials). Three gamble conditions were presented in a pseudorandom order: "Positive Skew" (25% probability of gaining $5.25 but 75% of losing $1.75), "Symmetric" (50% probability of gaining or losing $3.05), and "Negative Skew" (25% probability of losing −$5.25 but 75% probability of gaining +$1.75). Expected value ($\mu = \$0.00$) and variance ($\sigma^2 = 9.19$) were held constant across all gambles. Subjects received an endowment ($10.00) before entering the scanner plus their cumulative outcome in cash at the end of the experiment. To test the effect of domain (gain or loss) on trial-by-trial choice, the endowment was subtracted from current earnings. Preference for each gamble type was then calculated as the proportion of trials that subjects accepted each, and overall risk preference was similarly indexed by averaging these proportions across gamble types.

fMRI Acquisition and Analysis

Images were acquired with a 3T General Electric Discovery 750 scanner (GE), using a 32-channel head coil. Forty-six 2.9-mm thick slices (2.9-mm isotropic voxels, interleaved acquisition) extended axially from the mid-pons to the top of the skull. Whole-brain functional scans were acquired with a T2*-weighted gradient pulse sequence (TR = 2 s, TE = 24 ms, flip angle = 77). A high-resolution T1-weighted anatomical image was also collected using an axial fast spoiled grass sequence (TR = 7.2 ms, TE = 2.3 ms, flip = 12, 0.9 mm isotropic voxels) for co-registration of functional image and DWI data and for volume of interest specification. Functional imaging analyses were conducted using AFNI and followed previously described methods (Supplemental Information; Knutson and Greer, 2008).

Mean activity time courses of predicted volumes of interest were plotted and statistically compared with targeted t tests (Figure 2). Percent signal change

prior to gamble choice in each trial (i.e., the second volume acquisition in the trial) were included in a logistic regression model that used peak neural activity (in the NAcc, AIns, and MPFC) to predict trial-by-trial gamble choices, and subjects were modeled as random effects. Finally, bootstrapped mediation analyses were conducted to determine whether NAcc activity could statistically mediate the association of AIns-NAcc tract coherence with positive-skew preference (Figure 3).

DWI Acquisition and Analysis

DWI data were also acquired on the same 3T scanner and head coil. A dual-spin echo diffusion-weighted sequence was used to acquire 2-mm isotropic images in 96 diffusion directions (b = 2,500 s/mm^2; TE = 97.5 ms). Ten non-diffusion-weighted (b = 0) volumes were acquired. Preprocessing and probabilistic tractography followed previously described procedures (Supplemental Information; Tournier et al., 2007). After identification, tracts were statistically validated using LiFE with virtual lesions (Supplemental Information; Pestilli et al., 2014).

SUPPLEMENTAL INFORMATION

Supplemental Information includes Supplemental Experimental Procedures, four figures, and four tables and can be found with this article online at http://dx.doi.org/10.1016/j.neuron.2015.12.015.

AUTHOR CONTRIBUTIONS

B.K., G.R.S.-L., J.K.L., and F.P. designed the research. C.C.W. and G.R.S.-L. acquired the data. J.K.L., F.P., and B.K. analyzed the data. J.K.L., F.P., and B.K. wrote the paper.

ACKNOWLEDGMENTS

We thank Kiefer Katovich for assistance and three reviewers for suggestions. The research and authors were supported by grants from the FINRA Investor Education Foundation, the Stanford Neuroscience Institute NeuroChoice Initiative, and the NIH (T32-MH020006, UL1-TR001107, UL1-TR001108, KL2-TR001106, R01-EY015000, F32-AG039131, K99-AG042596, R00-AG042596).

Received: June 22, 2015
Revised: October 6, 2015
Accepted: December 8, 2015
Published: January 6, 2016

REFERENCES

Aron, A.R., Behrens, T.E., Smith, S., Frank, M.J., and Poldrack, R.A. (2007). Triangulating a cognitive control network using diffusion-weighted magnetic resonance imaging (MRI) and functional MRI. J. Neurosci. *27*, 3743–3752.

Basser, P.J., and Pierpaoli, C. (1996). Microstructural and physiological features of tissues elucidated by quantitative-diffusion-tensor MRI. J. Magn. Reson. B. *111*, 209–219.

Chang, L.J., Yarkoni, T., Khaw, M.W., and Sanfey, A.G. (2013). Decoding the role of the insula in human cognition: functional parcellation and large-scale reverse inference. Cereb. Cortex *23*, 739–749.

Chikama, M., McFarland, N.R., Amaral, D.G., and Haber, S.N. (1997). Insular cortical projections to functional regions of the striatum correlate with cortical cytoarchitectonic organization in the primate. J. Neurosci. *17*, 9686–9705.

Choi, J.K., Chen, Y.I., Hamel, E., and Jenkins, B.G. (2006). Brain hemodynamic changes mediated by dopamine receptors: Role of the cerebral microvasculature in dopamine-mediated neurovascular coupling. Neuroimage *30*, 700–712.

Clark, L., Bechara, A., Damasio, H., Aitken, M.R.F., Sahakian, B.J., and Robbins, T.W. (2008). Differential effects of insular and ventromedial prefrontal cortex lesions on risky decision-making. Brain *131*, 1311–1322.

Coenen, V.A., Panksepp, J., Hurwitz, T.A., Urbach, H., and Mädler, B. (2012). Human medial forebrain bundle (MFB) and anterior thalamic radiation (ATR): imaging of two major subcortical pathways and the dynamic balance of opposite affects in understanding depression. J. Neuropsychiatry Clin. Neurosci. *24*, 223–236.

Cohen, M.X., Schoene-Bake, J.C., Elger, C.E., and Weber, B. (2008). Connectivity-based segregation of the human striatum predicts personality characteristics. Nat. Neurosci. *15*, 29–30.

Craig, A.D. (2009). How do you feel—now? The anterior insula and human awareness. Nat. Rev. Neurosci. *10*, 59–70.

Critchley, H.D., Mathias, C.J., and Dolan, R.J. (2001). Neural activity in the human brain relating to uncertainty and arousal during anticipation. Neuron *29*, 537–545.

Draganski, B., Kherif, F., Klöppel, S., Cook, P.A., Alexander, D.C., Parker, G.J.M., Deichmann, R., Ashburner, J., and Frackowiak, R.S.J. (2008). Evidence for segregated and integrative connectivity patterns in the human Basal Ganglia. J. Neurosci. *28*, 7143–7152.

Haber, S.N., and Knutson, B. (2010). The reward circuit: linking primate anatomy and human imaging. Neuropsychopharmacology *35*, 4–26.

Heimer, L., Zahm, D.S., Churchill, L., Kalivas, P.W., and Wohltmann, C. (1991). Specificity in the projection patterns of accumbal core and shell in the rat. Neuroscience *41*, 89–125.

Jones, D.K., Knösche, T.R., and Turner, R. (2013). White matter integrity, fiber count, and other fallacies: the do's and don'ts of diffusion MRI. Neuroimage *73*, 239–254.

Kahneman, D., and Tversky, A. (1979). Prospect theory: An analysis of decision under risk. Econometrica *47*, 263–292.

Knutson, B., and Bossaerts, P. (2007). Neural antecedents of financial decisions. J. Neurosci. *27*, 8174–8177.

Knutson, B., and Gibbs, S.E.B. (2007). Linking nucleus accumbens dopamine and blood oxygenation. Psychopharmacology (Berl.) *191*, 813–822.

Knutson, B., and Greer, S.M. (2008). Anticipatory affect: neural correlates and consequences for choice. Philos. Trans. R. Soc. Lond. B Biol. Sci. *363*, 3771–3786.

Knutson, B., Katovich, K., and Suri, G. (2014). Inferring affect from fMRI data. Trends Cogn. Sci. *18*, 422–428.

Kraus, A., and Litzenberger, R.H. (1976). Skewness preference and the valuation of risk assets. J. Finance *31*, 1085–1100.

Kuhnen, C.M., and Knutson, B. (2005). The neural basis of financial risk taking. Neuron *47*, 763–770.

Lehéricy, S., Ducros, M., Van de Moortele, P.F., Francois, C., Thivard, L., Poupon, C., Swindale, N., Ugurbil, K., and Kim, D.S. (2004). Diffusion tensor fiber tracking shows distinct corticostriatal circuits in humans. Ann. Neurol. *55*, 522–529.

Lehman, J.F., Greenberg, B.D., McIntyre, C.C., Rasmussen, S.A., and Haber, S.N. (2011). Rules ventral prefrontal cortical axons use to reach their targets: implications for diffusion tensor imaging tractography and deep brain stimulation for psychiatric illness. J. Neurosci. *31*, 10392–10402.

Mohr, P.N.C., Biele, G., and Heekeren, H.R. (2010). Neural processing of risk. J. Neurosci. *30*, 6613–6619.

Palminteri, S., Justo, D., Jauffret, C., Pavlicek, B., Dauta, A., Delmaire, C., Czernecki, V., Karachi, C., Capelle, L., Durr, A., and Pessiglione, M. (2012). Critical roles for anterior insula and dorsal striatum in punishment-based avoidance learning. Neuron *76*, 998–1009.

Panksepp, J. (1998). Affective Neuroscience: The Foundations of Human and Animal Emotions (New York: Oxford University Press).

Paulus, M.P., Rogalsky, C., Simmons, A., Feinstein, J.S., and Stein, M.B. (2003). Increased activation in the right insula during risk-taking decision making is related to harm avoidance and neuroticism. Neuroimage *19*, 1439–1448.

Pestilli, F., Yeatman, J.D., Rokem, A., Kay, K.N., and Wandell, B.A. (2014). Evaluation and statistical inference for human connectomes. Nat. Methods *11*, 1058–1063.

Petrides, M., and Pandya, D.N. (2007). Efferent association pathways from the rostral prefrontal cortex in the macaque monkey. J. Neurosci. *27*, 11573–11586.

Reynolds, S.M., and Zahm, D.S. (2005). Specificity in the projections of prefrontal and insular cortex to ventral striatopallidum and the extended amygdala. J. Neurosci. *25*, 11757–11767.

Samanez-Larkin, G.R., and Knutson, B. (2015). Decision making in the ageing brain: changes in affective and motivational circuits. Nat. Rev. Neurosci. *16*, 278–289.

Samanez-Larkin, G.R., Levens, S.M., Perry, L.M., Dougherty, R.F., and Knutson, B. (2012). Frontostriatal white matter integrity mediates adult age differences in probabilistic reward learning. J. Neurosci. *32*, 5333–5337.

Sanfey, A.G. (2007). Social decision-making: insights from game theory and neuroscience. Science *318*, 598–602.

Tournier, J.D., Calamante, F., and Connelly, A. (2007). Robust determination of the fibre orientation distribution in diffusion MRI: non-negativity constrained super-resolved spherical deconvolution. Neuroimage *35*, 1459–1472.

von Neumann, J., and Morgenstern, O. (1944). Theory of Games and Economic Behavior (Princeton, NJ: Princeton University Press).

Wu, C.C., Bossaerts, P., and Knutson, B. (2011). The affective impact of financial skewness on neural activity and choice. PLoS ONE *6*, e16838.

Wu, C.C., Sacchet, M.D., and Knutson, B. (2012). Toward an affective neuroscience account of financial risk taking. Front. Neurosci. *6*, 159.

Neuron

Supplemental Information

White-Matter Tract Connecting Anterior Insula to Nucleus Accumbens Correlates with Reduced Preference for Positively Skewed Gambles

Josiah K. Leong, Franco Pestilli, Charlene C. Wu, Gregory R. Samanez-Larkin, and Brian Knutson

Supplemental Information

Supplemental Data

Supplemental Experimental Procedures

Supplemental Data
Figure S1. Related to Figure 1.

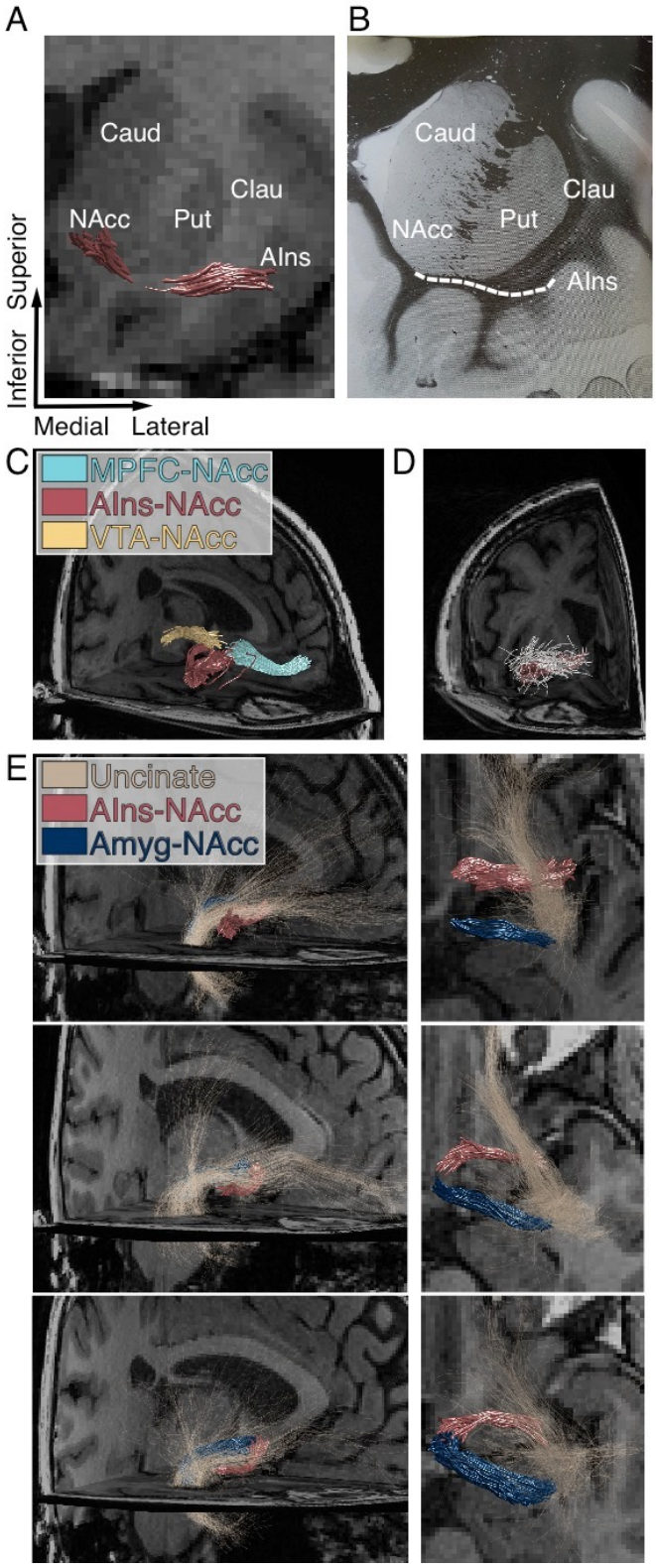

(A) AIns to NAcc tract traverses subcaudate white matter inferior to the claustrum and putamen, intersecting laterally with the uncinate fasciculus. Controlling for coherence of crossing fibers did not change the observed relations between AIns-NAcc tract coherence and age or behavior (see *Table S2*).
(B) Myelin-stained coronal slice of right hemisphere at level of the caudate head (NAcc=nucleus accumbens, Caud=caudate, Clau=claustrum, AIns=anterior insula, Put=putamen, adapted from Mai, Assheuer, and Paxinos, 1997).
(C) Reproduction of **Figure 1A** with the AIns-NAcc tract prior to removing outliers, as described in *Experimental Procedures*.
(D) Path-neighborhood fascicles from the whole-brain connectome for a representative subject's right AIns-NAcc tract. The fascicles which comprised the AIns-NAcc tract were included with these fascicles (as depicted) in the full model to predict raw diffusion signal. The "virtually lesioned" model included only the path-neighborhood fascicles. Root mean squared error of the predicted diffusion signal was compared to test the strength of evidence for the tract (see *Supplemental Experimental Procedures*).
(E) Sagittal and axial cross sections of three representative subjects' right AIns-NAcc tract, uncinate fasciculus, and amygdala-NAcc tract. Coherence of these tracts were entered as covariates of no interest in all regressions involving the AIns-NAcc tract (see *Table S3*). The AIns-NAcc tract passes ventrally through the uncinate fasciculus along the lateral-medial axis, and the pathways share a proportion of their voxels, (computed within subject then averaged between subjects: right mean=0.45, standard deviation=0.18, range=0.00-0.71; left mean=0.36, standard deviation=0.14, range=0.01-0.65).

Figure S2. Related to Figure 2.

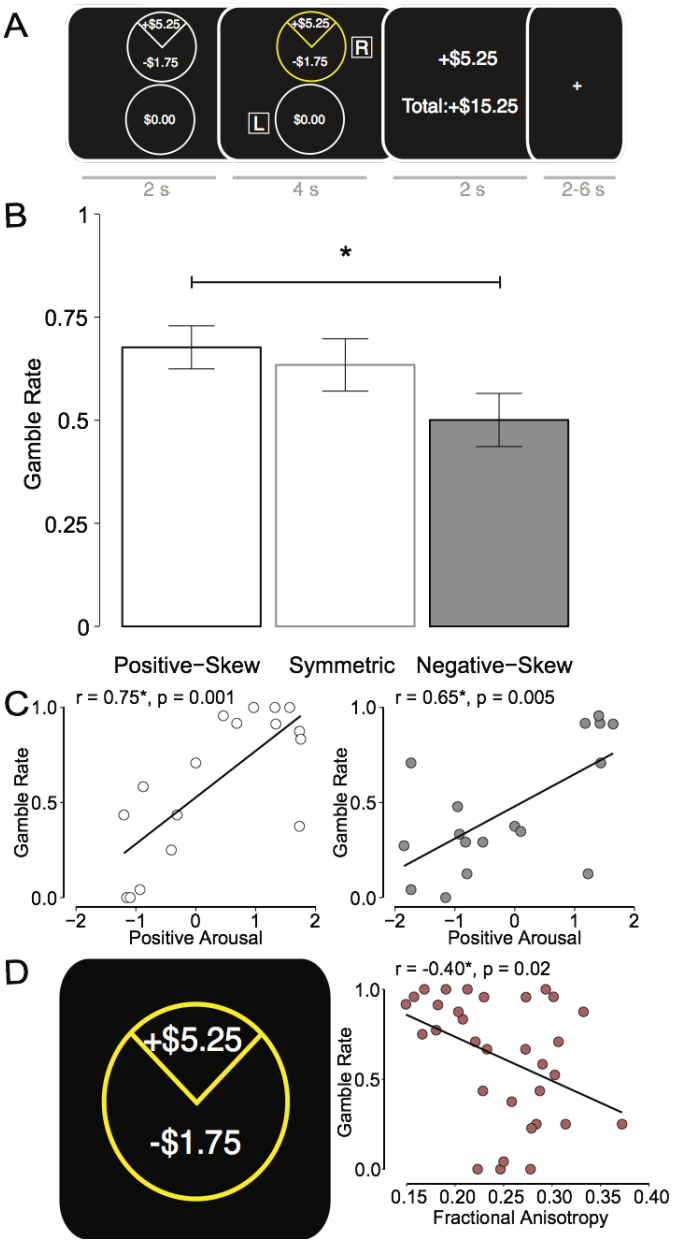

(A) Gambling task trial structure. Subjects passively viewed two gamble options (2 s), then chose between the gambles (4 s), saw the gamble outcome (2 s), and then fixated for a variable 2-6 s inter-trial interval until the next trial began (see *Experimental Procedures*).

(B) Risk seeking rate for each gamble condition. Mean gamble rate and standard error were computed for subjects who did not always seek or avoid risk for any gamble condition (n=20). Positively skewed gambles were preferred to negatively skewed gambles (paired t(19)=2.13, p=0.047).

(C) Subjects (n=17) rated each gamble type on a 7-point Likert scale for evoked valence (negative-positive) and arousal (low-high), after performing the gambling task (data loss due to a technical difficulty). Ratings were mean-deviated within subject, plotted along the two dimensions and rotated 45 degrees to derive affective measures of positive and negative arousal. Positive arousal ratings towards positively and negatively skewed gambles were highly correlated with risk seeking for each of those gambles (positive-skew: **β**=0.75, t(15)=4.40, p=0.0005; negative-skew: **β**=0.65, t(15)=3.32, p=0.005).

(D) Individual differences in right AIns-NAcc tract coherence was associated with decreased preference for positively skewed gambles (**β**=-0.40, t(30)=-2.38, p=0.02; see also *Table S1*).

Figure S3. Related to Figure 2.

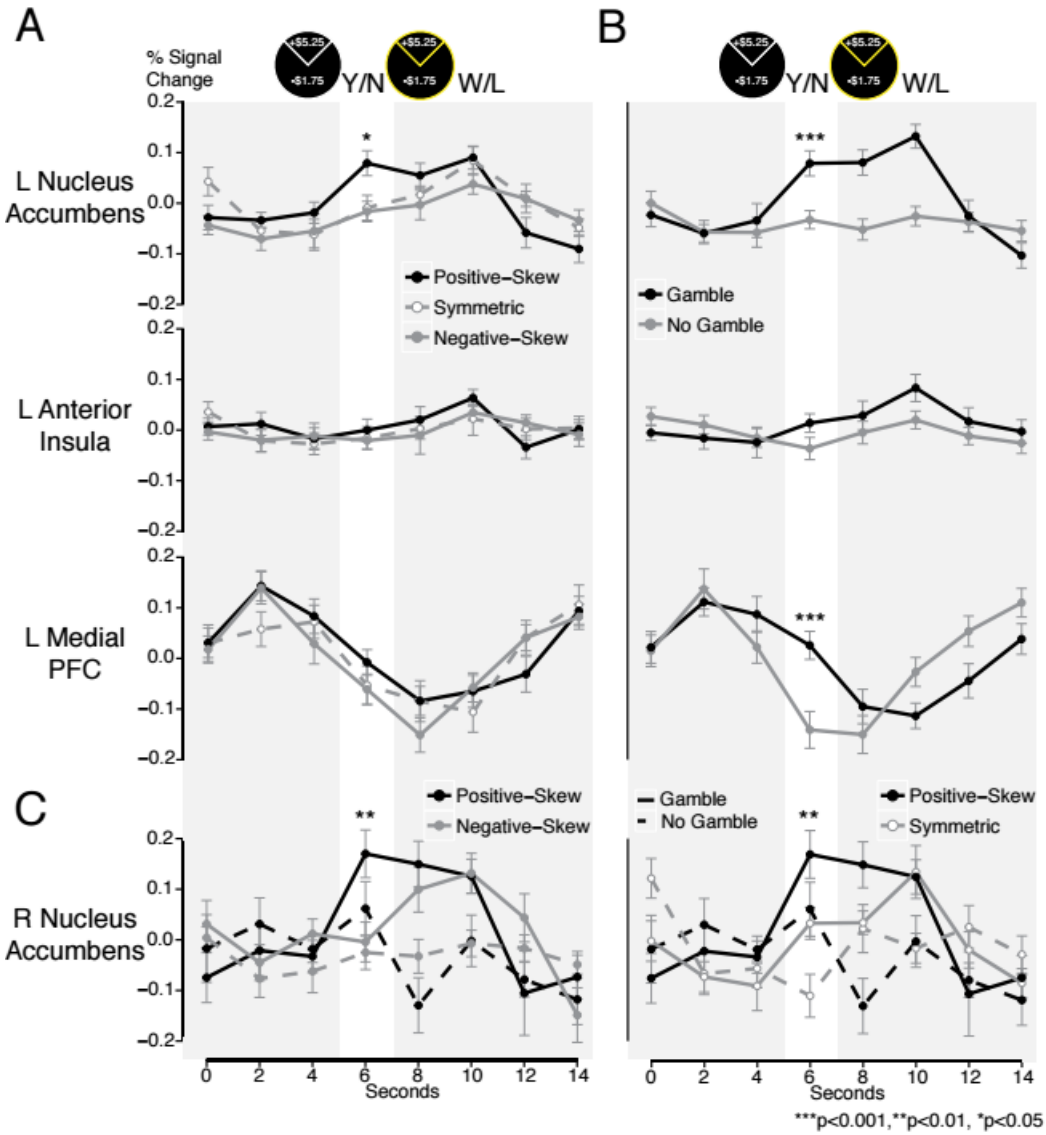

(A) Left hemisphere activity time courses showed a similar pattern of functional activity in each volume of interest (VOI) as the right hemisphere, with the same significant main effects. Presentation of positively skewed gambles elicited greatest NAcc activity (positive-skew > symmetric: paired t(31)=2.87, p=0.007; positive-skew > negative-skew: paired t(31)=3.02, p=0.005).

(B) Similar to right hemisphere, left NAcc and MPFC activity were greater prior to gamble acceptance than rejection across conditions (NAcc: paired t(31)=3.54, p=0.001; MPFC: paired t(31)=3.78, p=0.001).

(C) Right NAcc activity was greater during choice for accepted positive-skew than accepted negative-skew and accepted symmetric gambles (positive > negative: t(26)=3.07, p=0.005; positive > symmetric: t(28)=3.31, p=0.003).

Figure S4. Related to Figure 3.

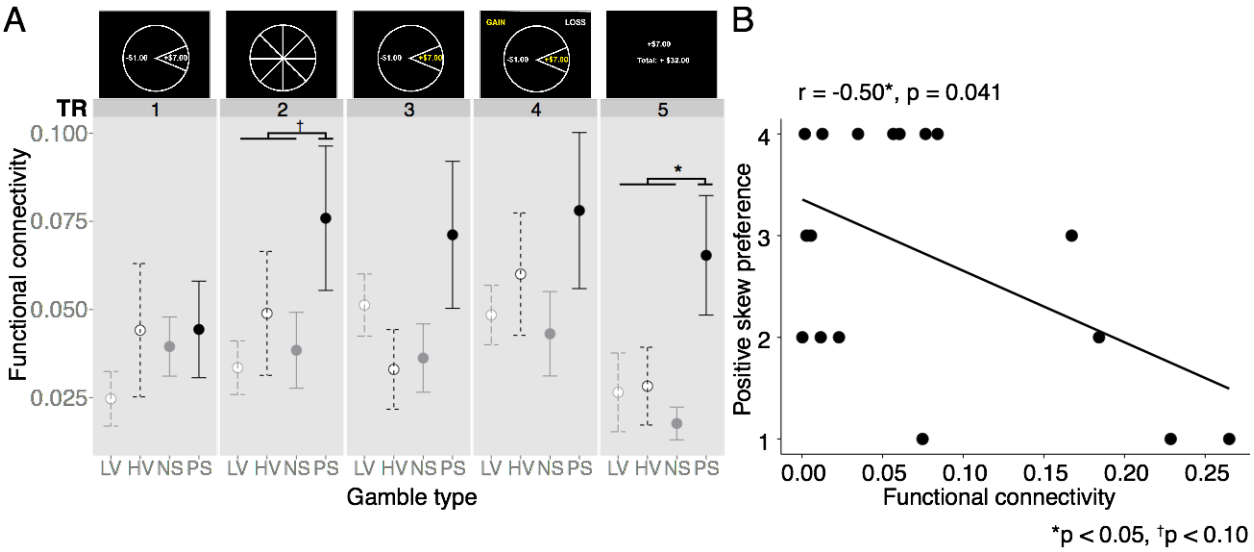

Confirmatory analyses were performed on previously published FMRI data (see Wu et al., 2011 for full experimental procedures). In that study, subjects (N=17) passively viewed gambles and their outcomes during FMRI. Subjects encountered four gamble types which were equated for expected value but differed in skewness: "Low-Variance" (LV), which yielded equal probability (50%) of winning or losing $1.00; "High-Variance" (HV), which yielded equal probability (50%) of winning or losing $2.75; "Negative-Skew" (NS), which yielded a low probability (12.5%) of losing a large amount (-$7.00) paired with a high probability (87.5%) of winning a small amount (+$1.00); "Positive-Skew" (PS), which yielded a low probability (12.5%) of winning a large amount (+ $7.00) paired with a high probability (87.5%) of losing a small amount (-$1.00). During each trial, subjects were presented a single gamble (2 s), saw the gamble spin randomly (2 s), saw the gamble outcome (2 s), responded to confirm they saw the outcome (2 s), and viewed their cumulative earnings for the task (2 s). After the experiment, subjects ranked the four gamble types in the order they would prefer to play them again. BOLD activity time courses were extracted from right hemisphere AIns and NAcc VOIs and lagged 6 seconds to account for the hemodynamic lag. The "functional connectivity" between the AIns and NAcc for each subject was assessed by performing simple linear regression between the two VOIs' activity for every phase of the trial (corresponding to volume acquisitions) and for each gamble type. The variance explained in the regression (r^2) was then averaged across subjects to extract a measure of functional connectivity for every trial phase and for each gamble type.

(A) Right AIns-NAcc functional connectivity was greater when subjects saw positively skewed gambles spin relative to all other gamble types with marginal significance (paired $t(16)=1.75$, $p<0.10$). Functional connectivity was also greatest while subjects viewed the outcomes of positively skewed gambles, relative to all other gambles (paired $t(16)=2.64$, $p=0.018$).

(B) Right AIns-NAcc functional connectivity while subjects saw the positively skewed gamble spin was used in individual difference analyses, and was associated with decreased preference for positively skewed gambles in post-scan ratings, ($\beta=0.50$, $t(15)=2.24$, $p=0.04$). FMRI data from the current study were analyzed the same way. Right AIns-NAcc functional connectivity before subjects chose to accept or reject gambles was greater for positively and negatively skewed gambles than for symmetric gambles (paired $t(31)=2.01$, $p=0.053$). In addition, right AIns-NAcc tract coherence was correlated with right AIns-NAcc functional connectivity when subjects first saw the prospective gambles for all gamble types (positive-skew: $\beta=0.47$, $t(30)=2.92$, $p=0.007$; symmetric: $\beta=0.41$, $t(30)=2.48$, $p=0.019$; negative-skew: $\beta=0.36$, $t(30)=2.13$, $p=0.041$; all coefficient estimates are standardized).

Table S1. Related to Figure 2.
An omnibus repeated-measures multivariate analysis of variance was performed by regressing the risk seeking rate for all three gamble conditions against all three bilateral tracts (six total tracts). This revealed a significant tract by gamble condition interaction for the AIns-NAcc tract bilaterally, and a significant difference in risk seeking by gamble condition. The significant interactions were examined in pairwise correlations described in the main text.

Variable	**Pillai's Trace**	**F-test**
AIns - NAcc (R)	0.265	F(1,25)=1.744, p=0.199
AIns - NAcc (L)	0.002	F(1,25)=0.011, p=0.916
MPFC - NAcc (R)	0.095	F(1,25)=0.626, p=0.437
MPFC - NAcc (L)	0.006	F(1,25)=0.042, p=0.840
VTA - NAcc (R)	0.044	F(1,25)=0.290, p=0.595
VTA - NAcc (L)	0.044	F(1,25)=0.289, p=0.596
Gamble condition	0.622	F(2,50)=4.016*, p=0.024
AIns - NAcc (R) * gamble condition	0.634	F(2,50)=4.097*, p=0.023
AIns - NAcc (L) * gamble condition	0.726	F(2,50)=4.688*, p=0.014
MPFC - NAcc (R) * gamble condition	0.012	F(2,50)=0.078, p=0.925
MPFC - NAcc (L) * gamble condition	0.021	F(2,50)=0.134, p=0.876
VTA - NAcc (R) * gamble condition	0.143	F(2,50)=0.921, p=0.405
VTA - NAcc (L) * gamble condition	0.257	F(2,50)=1.660, p=0.200

*$p<0.05$

Table S2. Related to Figure 1.
Uncinate fasciculus and amygdala-NAcc tract fractional anisotropy (FA) were included as covariates of no-interest in all regression analyses involving the right AIns-NAcc tract. All results remained statistically significant or marginally significant, while neither of the control tracts were significantly correlated with positive skew preference and NAcc activity. Coefficient estimates are standardized **β**s. The uncinate fasciculus was tracked using Automated Fiber Quantification (AFQ; Yeatman et al., 2012). The amygdala-NAcc tract was tracked using the same methods described in *Experimental Procedures*. The amygdala VOI for seeding in tractography was defined by FreeSurfer segmentation (Fischl et al., 2002).

Association	**Variable of interest**
AIns-NAcc FA ~ Age + Uncinate fasciculus FA + Amygdala-NAcc FA	Age: **β**=0.56**, p=0.001
Positive skew preference ~ AIns-NAcc FA + Uncinate fasciculus FA + Amygdala-NAcc FA	AIns-NAcc: **β**=-0.36*, p=0.039
NAcc activity ~ AIns-NAcc FA + Uncinate fasciculus FA + Amygdala-NAcc FA	AIns-NAcc: **β**=-0.32†, p=0.072

**p<0.01, *p<0.05, †<0.10

Table S3. Related to Table 1.
Including left hemisphere neural activity did not improve model fit (as indexed by AIC, BIC, and a likelihood-ratio test: $\chi^2(3)=1.52$, $p=0.68$) for logistic regression models predicting behavior (subjects included as random effects).

Variables	Contrasts	Right VOIs model	Left VOIs model	Bilateral VOIs model
Previous Gamble	Win > Loss	-2.55* [-0.17, 0.07]	-2.35* [-0.15, 0.06]	-2.54* [-0.17, 0.07]
	Accept > Reject	2.01* [0.18, 0.09]	1.96* [0.17, 0.09]	2.05* [0.18, 0.09]
Domain of current earnings	Loss	1.71 [0.45, 0.26]	1.58 [0.42, 0.26]	1.70 [0.45, 0.26]
	Gain	1.52 [0.39, 0.26]	1.39 [0.36, 0.26]	1.51 [0.39, 0.26]
Skewness	Positive > Negative	5.50*** [0.32, 0.06]	5.73*** [0.34, 0.06]	5.44*** [0.32, 0.06]
	Skewed > Symmetric	-5.86*** [-0.52, 0.09]	-5.92*** [-0.52, 0.09]	-5.90*** [-0.52, 0.09]
Right NAcc		5.09*** [0.67, 0.13]		3.01** [0.54, 0.18]
Right AIns		-3.00** [-0.36, 0.12]		-2.91** [-0.38, 0.13]
Right MPFC		3.50*** [0.34, 0.10]		2.01* [0.28, 0.14]
Left NAcc			3.87*** [0.49, 0.13]	1.09 [0.19, 0.17]
Left AIns			-0.72 [-0.11, 0.15]	-0.22 [-0.04, 0.16]
Left MPFC			2.49** [0.22, 0.09]	0.54 [0.07, 0.14]
Pseudo R^2		0.30	0.29	0.30
AIC		2594	2612	2599
BIC		2657	2675	2679

Z-scores with coefficient estimates and SE in parentheses. ***p<0.001, **p<0.01, *p<0.05

Table S4. Related to Figure 3.
Additional mediation models verified that only right NAcc activity mediated the relation between right AIns-NAcc tract fractional anisotropy (FA) and positive skew preference. Path coefficients are standardized **β**s.

	a Structure ➞ Function	b Function ➞ Behavior	c'/c Structure ➞ Behavior
R AIns-NAcc FA ➞ R NAcc ➞ Positive-Skew	-0.35* (p=0.03)	0.46** (p<0.01)	c'=-0.24 (p=0.14) c=-0.40* (p=0.02)
R AIns-NAcc FA ➞ R AIns ➞ Positive-Skew	-0.07 (p=0.63)	0.12 (p=0.52)	c'=-0.39* (p<0.01) c=-0.40* (p=0.02)
R AIns-NAcc FA ➞ R MPFC ➞ Positive-Skew	-0.38* (p=0.01)	0.19 (p=0.28)	c'=-0.33* (p=0.03) c=-0.40* (p=0.02)
R MPFC-NAcc FA ➞ R NAcc ➞ Positive-Skew	-0.18 (p=0.27)	0.52*** (p<0.001)	c'=-0.10 (p=0.55) c=-0.19 (p=0.29)
R MPFC-NAcc FA ➞ R MPFC ➞ Positive-Skew	-0.21 (p=0.22)	0.28 (p=0.09)	c'=-0.14 (p=0.45) c=-0.19 (p=0.29)

***p<0.001; **p<0.01; *p<0.05

Supplemental Experimental Procedures

Reliability of risk preferences.

To verify the temporal stability of gamble choice as a measure of individual differences in risk preferences, we calculated the reliability of choices for each gamble condition across the experiment (see *Figure S2* and *Experimental Procedures*). Split-half reliability estimates indicated significant internal consistency in risk preference within each gamble condition and overall (positive-skew: ICC=0.89, $p<0.0001$; symmetric: ICC=0.91, $p<0.0001$; negative-skew: ICC=0.93, $p<0.0001$; overall: ICC=0.94, $p<0.0001$).

FMRI analysis.

For preprocessing, individual subject data were sinc interpolated to correct for non-simultaneous slice acquisition, corrected for motion in six dimensions, spatially smoothed using a small kernel (full width at half maximum=4 mm), and high-pass filtered (omitting frequencies with period < 90 s). Visual inspection of motion correction estimates confirmed that five subjects' heads had moved more than 2 mm in a plane from one whole-brain volume acquisition to the next, and these were excluded from further analysis.

To obtain activity time courses for targeted analyses, spherical volumes of interest (VOIs; 8 mm diameter) were centered on bilateral foci for the NAcc (Talairach coordinates: +/10,12,-2), AIns (Talairach coordinates: +/-34,24,-4), and MPFC (Talairach coordinates: +/-4,45,0), based on previous literature (Genevsky et al., 2013; Knutson and Greer, 2008). VOIs were warped from Talairach space to subjects' native brain space, and activity was spatially averaged within each VOI and then divided by the mean activity over the entire experiment to derive continuous measures of percent signal change. Time courses were then lagged 2 volume acquisitions (or 4 s) to account for the hemodynamic response delay to peak response.

DWI analysis.

For preprocessing, anatomical landmarks were manually defined in the anterior and posterior commissures (AC-PC), and the midsagittal plane to guide a rigid-body transformation that converted the T1-weighted images into AC-PC aligned space. Eddy-current distortions and subject motion in the diffusion-weighted images were corrected by a 14-parameter constrained non-linear co-registration based on expected eddy-current distortions, given the phase-encode direction of acquired data. Each diffusion-weighted image was registered to the mean of the motion-corrected non-diffusion-weighted (b = 0) images. The mean of the non-diffusion-weighted images was aligned to the T1 image in AC-PC space using a rigid body transformation. All raw diffusion images were resampled to 2 mm isotropic voxels by combining motion correction, eddy-current correction, and anatomical alignment into one general transformation, and then resampling the data using a seventh-order b-spline algorithm. Preprocessing was performed using the open-source mrDiffusion package (www.github.com/vistalab/vistasoft).

To define anatomical VOIs, each subject's AC-PC aligned T1-weighted image was processed with FreeSurfer software (http://surfer.nmr.mgh.harvard.edu/, Fischl, 2012). NAcc VOIs were identified from probabilistic subcortical tissue classification based on a manually labeled training set (Fischl et al., 2002). AIns VOIs were derived from the Destrieux cortical parcellation atlas, by combining the anterior insula and short gyrus parcellations (Destrieux et al., 2010). A binary mask was formed using the white versus gray-matter border identified by FreeSurfer to restrict fibers to the white-matter volume. To track previously described tracts of interest, spherical VOIs (8 mm diameter) were manually placed in bilateral MPFC and VTA, as described in previous research (Samanez-Larkin et al., 2012).

Probabilistic tractography.

Fiber tracking between AIns and NAcc VOIs was performed using constrained spherical deconvolution based probabilistic tracking, as implemented in MRtrix software (Tournier et al., 2007). The maximum number of harmonics was set to 10 (L_{max}=10), which defined the maximum number of deconvolution kernels utilized by constrained spherical deconvolution to estimate the fiber orientation distribution function in each voxel. This required 66 parameters for fitting the function (or 30 less than the 96 measured diffusion directions). Fiber pathways were generated by randomly seeding a voxel in a starting VOI and tracking until the fiber reached the ending VOI (step size=0.2 mm; minimum length=10 mm; maximum length=200 mm; minimum radius of curvature=1 mm; FA amplitude cutoff = 0.075; initial cutoff = 0.05). Fibers leaving the white-matter volume were discarded. Fiber tracking was also conducted on previously described mesolimbic tracts of interest between MPFC and NAcc VOIs, as well as VTA and NAcc VOIs (Samanez-Larkin et al., 2012). To ensure comparability with previous research, the same probabilistic tractography algorithm was again used to track these pathways in the current study (ConTrack; Sherbondy et al., 2008). A set of 50,000 candidate fibers connecting the VOI pairs were identified in each hemisphere. Seeds were placed randomly in both VOIs to ensure symmetric tracking. Candidate fibers were scored

using the ConTrack scoring algorithm, and the top-scoring 1% (which putatively tracked the most likely connecting pathways) were retained.

Fibers obtained from all tractography solutions were reduced to core fiber bundles by eliminating outliers and anatomically unlikely pathways (e.g., fibers crossing the cerebral hemispheres). Specifically, fibers greater than 2 standard deviations from the mean fiber length were initially removed. Fibers greater than 3 standard deviations away from the mean position of the core fiber (Mahalanobis distance) were then removed. Finally, fibers that crossed the midsagittal plane or took indirect routes between VOIs were removed (e.g., those that projected in one direction, but then looped backward). The proportions of fibers removed from each tract, averaged across subjects, were: right AIns-NAcc: 0.61, left AIns-NAcc: 0.54, right MPFC-NAcc: 0.31, left MPFC-NAcc: 0.30, right VTA-NAcc: 0.61, left VTA-NAcc: 0.62. These proportions were similar to the proportion of fibers discarded for previously characterized tracts using the same method (e.g., right uncinate: 0.59, left uncinate: 0.64, right amygdala-NAcc: 0.49, left amygdala-NAcc: 0.47; see also *Figure S1*).

Tract validation.

Linear Fascicle Evaluation (LiFE) is a forward modeling approach that predicts the raw measured diffusion signal by generating a synthetic signal using all of the discovered fascicles in the white-matter brain volume. A weight is assigned to each fascicle in a connectome by computing the root mean squared error difference between measured and predicted signal. Many fascicles are deleted during this process and not considered for further anatomical analysis. To statistically validate surviving fascicles, those forming a tract of interest (e.g., the AIns to NAcc tract) are removed from the connectome by a "virtual lesion". The resulting "lesioned" connectome should have increased root mean squared error, which can be compared to the error of the unlesioned connectome. The strength of evidence in favor of a tract is measured as the increase in root mean squared error between the lesioned and unlesioned connectome. Thus, this analytic procedure shares similarity with power analysis and can quantify the statistical evidence for a specific tract, given the measured whole brain diffusion signal and the estimated fascicles.

To validate tracts of interest, we first tracked a whole-brain connectome by applying the same parameters used for the AIns to NAcc tract to a whole-brain seed mask. Next, we specifically evaluated the difference in error in the set of voxels that intersected with the tract of interest. Fascicles from the whole-brain connectome that passed through at least one of the voxels were designated as path-neighborhood fascicles (Wedeen et al., 2012; *Figure S1*). We calculated the root mean squared error of the predicted diffusion signal in each voxel using the full unlesioned model (including path-neighborhood and tract of interest fascicles), as well as root mean squared error for a reduced model (a virtual lesion model that included only the path-neighborhood fibers). The strength of the evidence favoring the existence of a tract of interest was calculated as the difference in the full minus reduced model mean prediction errors (μ) divided by their pooled standard deviations (**Figure 1B**).

The strength of evidence (*S*) returns a scalar value bounded at zero and infinity. We used this value for group statistics across individual brains, and tested that the mean strength of evidence (*S*) was greater than zero (methods detailed in Gomez et al., 2015; Pestilli, 2015, Pestilli et al., 2014, and Takemura et al., 2015; francopestilli.github.io/life).

For identified tracts, one-sample Wilcoxon signed-rank tests compared the mean strength of evidence (log-transformed to unbound the distribution of values from $-\infty$ to $+\infty$) against the null hypothesis of no evidence for the tracts ($\mu = 0$), and indicated significant strength of evidence for all tracts (right AIns-NAcc: $V=528$, $p<0.001$; left AIns-NAcc: $V=523$, $p<0.001$; right MPFC-NAcc: $V=528$, $p<0.001$; left MPFC-NAcc: $V=528$, $p<0.001$; right VTA-NAcc: $V=528$, $p<0.001$; left VTA-NAcc: $V=471$, $p<0.001$; see also *Figure S1*).

Diffusion index calculation.

Diffusion properties of validated tracts were characterized by obtaining mean fractional anisotropy (FA) for each tract, which can vary as a function of fascicle density, axon diameter, and myelination. To assess variation in FA along the trajectory of each tract, we spatially normalized fiber pathways between subjects by sampling 100 evenly spaced cross-sectional nodes along the tract length from the starting VOI to the ending VOI. The mean FA in each node was then calculated as an average of each fiber's FA in that node, weighted by the spatial distance of that fiber from the node's core fiber. We then averaged FA across the middle 50% of nodes along each pathway to ensure that FA measures exclusively included white matter, but not voxels along the gray versus white-matter boundary. This generated a single FA (or "coherence") value for each tract in each hemisphere of every subject (see also Yeatman et al., 2012). These measures robustly correlated across hemispheres (AIns-NAcc: $r=0.59$, $F(1,30)=15.89$, $p<0.001$; MPFC-NAcc: $r=0.79$, $F(1,30)=50.89$, $p<0.001$; VTA-NAcc: $r=0.82$, $F(1,30)=61.01$, $p<0.001$).

Replication and extension of previously identified associations of tract coherence with age.

Results from this new dataset replicated a previously documented negative association of age with bilateral MPFC-NAcc tract coherence (β=-0.53, $t(30)=-3.42$, $p=0.002$), as well as a marginally positive association of age with

bilateral VTA-NAcc tract coherence (**β**=0.35, t(30)=2.03, p=0.051; see **Figure 1D** in main paper; Samanez-Larkin, et al., 2012). Like VTA-NAcc tract coherence, age was positively associated with AIns-NAcc tract coherence in both hemispheres, (right: **β**=0.42, t(30)=2.52, p=0.02; left: **β**=0.45, t(30)=2.79, p=0.01; bilateral: **β**=0.49, t(30)=3.07, p=0.005; all coefficient estimates are standardized).

These findings also replicated specific age correlates of the coherence of these tracts, since MPFC to NAcc tract coherence was negatively correlated with age, but projections connecting the midbrain and the NAcc were not (Samanez-Larkin et al., 2012). Interpreting the properties of mesolimbic midbrain to NAcc projections poses a challenge than putative unidirectional glutamatergic MPFC to NAcc and AIns to NAcc projections, since the mesolimbic tract contains neurochemically varied and bidirectional projections traversed by numerous crossing fibers (Nieuwenhuys, 1985). Nonetheless, several reports using diffusion weighted tractography have now traced the trajectory of mesolimbic projections (Bracht et al., 2014; Coenen et al., 2012; Samanez-Larkin et al., 2012), and future combination with comparative techniques may better disentangle contributions of different components of this tract (e.g., Lammel et al., 2011). As with the midbrain to NAcc tract, age was positively correlated with the coherence of the AIns to NAcc tract. While unexpected, this association deserves further replication and exploration, particularly with respect to physiological mechanisms responsible for age-related decreases in the coherence in prefrontal but not subcortical tracts, their plasticity, and implications for function.

Distinguishing alternative tracts.

Since the AIns-NAcc tract and uncinate fasciculus share a proportion of voxels in some (but not all) subjects, the current methods cannot dissociate their diffusion characteristics in intersecting voxels. To partially address this issue, fractional anisotropy of the uncinate fasciculus was assessed and included as a covariate in all regressions involving the right AIns-NAcc tract, but could not statistically account for the results (see *Table S2*). The nearby ventral amygdalofugal pathway connecting the amygdala to the NAcc was also tracked using the current methods, and shown to terminate in posterior NAcc without intersecting with the more anterior AIns-NAcc tract (see *Figure S1*). The amygdala-NAcc tract also courses through the uncinate fasciculus, following the same superior trajectory as the uncinate in the inferior temporal cortex (Petrides and Pandya, 2007), but then diverging medially near the edge of the insula. These amygdalar projections are considered as distinct from the uncinate tract (Ungerleider, Gaffan, and Pelak, 1989). Amygdala-NAcc tract fractional anisotropy was also included with uncinate fractional anisotropy as a covariate in all regressions, and similarly could not statistically account for the AIns-NAcc tract results (see *Table S2*). Together, these additional analyses suggest that the AIns-NAcc tract is at least partially distinct from other nearby tracts, but further verification of this distinction will have to await the development of more sophisticated methods for teasing apart different but overlapping tracts.

Supplemental References

Bracht, T., Doidge, A. N., Keedwell, P. A., and Jones, D. K. (2015). Hedonic tone is associated with left superflo-lateral medial forebrain bundle microstructure. *Psychol Med*, *45*, 865-874.

Destrieux, C., Fischl, B., Dale, A., and Halgren, E. (2010). Automatic parcellation of human cortical gyri and sulci using standard anatomical nomenclature. *NeuroImage*, *53*(1), 1–15.

Fischl, B. (2012). FreeSurfer. *Neuroimage*, *62*(2), 774-781.

Fischl, B., Salat, D.H., Busa, E., Albert, M., Dieterich, M., Haselgrove, C., van der Kouwe, A., Killiany, R., Kennedy, D., Klaveness, S., Montillo, A., Makris, N., Rosen, B., and Dale, A.M. (2002). Whole brain segmentation: automated labeling of neuroanatomical structures in the human brain. *Neuron*, 33, 341-355.

Genevsky, A., Västfjäll, D., Slovic, P., and Knutson, B. (2013). Neural underpinnings of the identifiable victim effect: affect shifts preferences for giving. *The Journal of Neuroscience*, *33*(43), 17188–17196.

Gomez, J., Pestilli, F., Witthoft, N., Golijeh, G., Liberman, A., Poltoratski, S., Yoon, J., and Grill-Spector, K. (2015). Functionally defined white matter reveals segregated pathways in human ventral temporal cortex associated with category-specificity. *Neuron*, *85*(1), 216–227.

Lammel, S., Ion, D. I., Roeper, J., and Malenka, R. C. (2011). Projection-specific modulation of dopamine neuron synapses by aversive and rewarding stimuli. *Neuron*, *70*(5), 855-862.

Mai, J.K., Assheuer, J., Paxinos, G. (1997). Atlas of the human brain (San Diego: Academic Press).

Nieuwenhuys, R. (1985). Chemoarchitecture of the Brain. SpringerVerlag, New York.

Pestilli, F. (2015). Test-retest measurements and digital validation for in vivo neuroscience. *Scientific Data*, *2*, 140057.

Petrides, M., and Pandya, D.N. (2007). Efference Association Pathways from the rostral Prefrontal Cortex in the Macaque Monkey. *The Journal of Neuroscience*, 27(43): 11573-11586.

Sherbondy, A.J., Dougherty, R.F., Ben-shachar, M., and Wandell, B.A. (2008). ConTrack: Finding the most likely pathways between brain regions using diffusion tractography. *Journal of Vision*, *8*(9), 1-16.

Takemura, H., Rokem, A., Winawer, J., Yeatman, J.D., Wandell, B.A., and Pestilli, F. (2015). A major human white matter pathway between dorsal and ventral visual cortex. *Cerebral Cortex*, published online March 31, 2015, doi: 10.1093/cercor/bhv064

Ungerleider, L.G., Gaffan, D., and Pelak, V.S. (1989). Projections from the inferior temporal cortex to prefrontal cortex via the uncinate fascicle in rhesus monkeys. *Experimental Brain Research*, 76: 473-484.

Wedeen, V.J., Rosene, D.L., Wang, R., Dai, G., Mortazavi, F., Hagmann, P., Kaas, J.H., and Tseng, W.I. (2012). The geometric structure of the brain fiber pathways. *Science*, *335*(6076), 1628-1634.